Author's personal copy

International Journal of Rock Mechanics & Mining Sciences 46 (2009) 855–864

Contents lists available at ScienceDirect

International Journal of Rock Mechanics & Mining Sciences

journal homepage: www.elsevier.com/locate/ijrmms

Thermal–hydrologic–mechanical–chemical processes in the evolution of engineered geothermal reservoirs

Joshua Taron *, Derek Elsworth

Department of Energy and Mineral Engineering and Center for Geomechanics, Geofluids, and Geohazards (G3), Pennsylvania State University, University Park, PA, USA

ARTICLE INFO

Article history:
Received 28 October 2008
Accepted 20 January 2009
Available online 27 February 2009

Keywords:
THMC
Geothermal simulation
Fracture reactive transport
Reservoir permeability
Dual porosity

ABSTRACT

In a companion paper [Taron J, Elsworth D, Min K-B. Numerical simulation of thermal–hydrologic–mechanical–chemical processes in deformable, fractured porous media. Int J Rock Mech Min Sci 2009; doi:10.1016/j.ijrmms.2009.01.008] we introduced a new methodology and numerical simulator for the modeling of thermal–hydrologic–mechanical–chemical processes in dual-porosity media. In this paper we utilize the model to examine some of the dominant behaviors and permeability-altering mechanisms that may operate in naturally fractured media. Permeability and porosity are modified as fracture apertures dilate or contract under the influence of pressure solution, thermo–hydro-mechanical compaction/dilation, and mineral precipitation/dissolution. We examine a prototypical enhanced geothermal system (EGS) for the relative, temporal arrival of hydro-mechanical vs. thermo-mechanical vs. chemical changes in fluid transmission as cold (70 °C) water is injected at geochemical disequilibrium within a heated reservoir (275 °C). For an injection-withdrawal doublet separated by ~670 m, the results demonstrate the strong influence of mechanical effects in the short-term (several days), the influence of thermal effects in the intermediate term (<1 month at injection), and the prolonged and long-term (>1 year) influence of chemical effects, especially close to injection. In most of the reservoir, cooling enhances permeability and increases fluid circulation under pressure-drive. We observe thermo-mechanical driven permeability enhancement in front of the advancing thermal sweep, counteracted by the re-precipitation of minerals previously dissolved into the cool injection water. Near injection, calcite dissolution is capable of increasing permeability by nearly an order of magnitude, while precipitation of amorphous silica onsets more slowly and can completely counteract this increase over the very long-term (>10 years). For the reinjection of highly-silica-saturated water, amorphous silica is capable of drastic reduction in permeability close to the injection well. With combined action from all mechanisms, permeability change varies by two orders of magnitude between injection and withdrawal.

© 2009 Elsevier Ltd. All rights reserved.

1. Introduction

In enhanced geothermal systems (EGS), as in reservoirs for the sequestration of CO_2, radioactive waste repositories, petroleum reservoirs, and other subsurface engineered facilities, fluid circulation is influenced in both the short- and long-term by chemical reaction and thermal-hydro-mechanical deformation. These forces operate upon temporally dynamic and spatially variable fluid transport properties, such as permeability, porosity, and fracture interconnectivity.

There are many considerations in the design of EGS, and most relate to the behavior of fractures. These include the potential for short-circuiting, the evolution of heat transfer surface area and of fluid residence time, working-fluid losses, and larger environmental concerns such as induced seismicity. Many processes are active in this regard. Some *inhibit* fluid transmission in dominant fractures, such as thin-film pressure solution [2–6], mineral precipitation [7–9], and thermo-mechanical aperture closure or creep. Others *enhance* transmission, such as shear dilation [10,11], mineral dissolution, force of crystallization [12–14], and strain energy driven free-face dissolution [5,6], while shear and dilation on existing and growing fractures is considered the primary contributor to induced seismicity [15].

Simulating these behaviors currently requires a staged approach, with some of the behaviors encompassed in thermal–-hydraulic (TH) or thermal–hydraulic–mechanical (THM) simulations, and others by thermal–hydraulic–chemical (THC) simulations. This may be adequate for many needs, but leaves out the rational and desirable linkage between chemical and mechanical behaviors. Pressure solution is by definition a chemical–mechanical process, as is free-face dissolution.

* Corresponding author. Tel.: +1 814 863 9733; fax: +1 814 865 3248.
E-mail address: jmt269@psu.edu (J. Taron).

1365-1609/$ - see front matter © 2009 Elsevier Ltd. All rights reserved.
doi:10.1016/j.ijrmms.2009.01.007

Author's personal copy

Other behaviors may, at first glance, seem adequately addressed through THM modeling, such as shear dilation and thermo-mechanical aperture closure. It is unclear, however, how such processes will be influenced by the action of chemical or chemo-mechanical mechanisms. For instance, aperture changes due to pressure solution result in the growth of contact area between fracture planes, and this in turn affects fracture shear strength and dilation angle. Alternatively, mineral precipitation/dissolution can alter the apertures of fractures, causing shifts in fluid and thermal flow paths that upset the stress condition and modify mechanical aperture. To examine these and other linkages, we introduce a modeling structure [1] that couples chemical and mechanical behaviors in a manner that reflects their interdependence on thermal and hydraulic effects (THMC). We apply this simulator to address some of the important questions in a prototypical EGS and, indeed, to examine the importance of these couplings and the strength of their interaction.

We first provide a brief overview of the approach and a description of the geological domain. A description of the chemical system and a simplified examination of injection water chemistry then follow to set the stage for further analysis. This is followed by an assessment of the relative, temporal arrival of hydro-mechanical vs. thermo-mechanical vs. chemical changes in fluid transmission and a recast of these in terms of characteristic times. Next, and perhaps most importantly, we evaluate the necessity for the explicit coupling of reactive transport to geomechanical processes and quantify the strength of coupling between independent processes. Finally, we follow the evolution of deviatoric stress in the reservoir and indicate locations most likely to undergo shearing failure.

2. Simulation mechanism

The simulations presented in the following utilize a newly developed THMC simulator [1] that couples the multiphase, multi-component, non-isothermal thermodynamics, reactive transport, and chemical precipitation/dissolution capabilities of TOUGHREACT [7] with the stress/deformation analyses FLAC^{3D} [16]. The coupled model incorporates features unique to fractured reservoirs (particularly those under elevated temperature and chemical potential), involving the undrained pressure response in a dual-porosity medium and with chemo-mechanical effects on deformation and on transport.

This "modular" approach, first proposed by Settari [17] to couple geomechanics with reservoir flow simulation, has some advantages over the development of a single coupled program. Modular approaches take advantage of the high state of development, sophistication, and validation available in purpose-build codes. The appropriate linking of codes which represent different behaviors—in this case those of solid mechanics and fluid transport—enables complex coupled processes to be represented and their interaction explored. With the appropriate choice of linking parameters and with the use of flexibly defined mesh overlays, the interaction of complex coupled processes may be explored with reasonable confidence and with rapid development.

Additionally, the modular construction [17,18] allows for easier implementation of future advances in constitutive or modeling technology (rather than modifying an entire coding structure), although typically the codes are not optimized to perform interactively, and may execute slowly; in our experience lowering computational efficiency due to the time required for data transfer between modules. As suggested by Settari and Mourits [18] and Minkoff et al. [19], however, this may not always be the case, because in systems where geomechanics may be loosely coupled (not changing at a rapid pace) the geomechanics simulation may not need to be conducted very often, thus improving computational efficiency over fully coupled codes where mechanics are equilibrated at every fluid flow time step.

FLAC^{3D} is exercised purely in mechanical mode, where undrained fluid pressures may be evaluated (externally) from local total stresses. This undrained methodology allows calculation of the short-time build-up in fluid pressures that results from an instantaneous change in stress, provided we have knowledge of the compressibility of the pore fluids and the solid matrix. In this way, the complex thermodynamics of phase equilibria of multiphase water mixtures, and even multi-component mixtures (such as CO_2 and water), can be tracked in the pre-existing framework of TOUGHREACT. For water mixtures, we utilize the 1997 International Association for the Properties of Water and Steam (IAPWS) steam table equations [20] to calculate fluid compressibility. If a system is unsaturated (such as in HDR) fluid compressibility is large, and the undrained poroelastic equations approach their drained counterparts. Therefore, while our construct is tailored to saturated systems, drained ones are automatically accommodated.

Sequential execution of the two programs is linked by a separate code, referred to as the "interpolation module", capable of parsing data outputs from each primary simulator as input to the companion. This module is a Fortran 90 executable, and maintains access to data outputs from TOUGHREACT and FLAC^{3D}. In addition to data interpolation, the module executes constitutive relationships including permeability evolution, dual-porosity poroelastic response to stress, and thermodynamically controlled fluid compressibility.

3. THMC permeability changes

The modeling structure calculates permeability change from the combined action of pressure solution, thermo-mechanical dilation/contraction, hydro-mechanical dilation/compaction, and bulk volume precipitation/dissolution of mineral species, with each depending intrinsically on temperature, effective stress, and chemical potential. Several methodologies could be used to model these behaviors; in the following we utilize laboratory results of fracture behavior under hydrothermal conditions to constrain in a single constitutive relationship the first three mechanisms. Compaction of fracture asperities is governed by [21]

$$b_{mc} = b_m^r + \{b_m^r - b_c^r + b_m^{\max} \exp(-\omega\sigma') \cdot \exp(-\sigma'(\beta - \chi/T)), \quad (1)$$

where b_{mc} is the fracture aperture at a given temperature, T, and effective stress, σ'. The residual (minimum possible) aperture at extreme mechanical stress is given by b_m^r, and at extreme chemical stress by b_c^r. The maximum possible aperture change is $b_m^{\max}$ (or the difference between initial and residual aperture), and the empirical coefficients that must be fit to laboratory data are β, χ, and ω, and represent the chemical, thermal, and mechanical dependence of the aperture, respectively (with ω representing non-linear fracture stiffness). This relationship has been previously compared to laboratory data [1,21].

Unloading (gaping) of the fracture is controlled by [1, modified from 21]

$$b_{m(u)} = b_{mc}(\sigma'_{\max}) + R_m b_m^{\max}\{\exp(-\omega\sigma') - \exp(-\omega\sigma'_{\max})\}, \quad (2)$$

where $b_{mc}(\sigma'_{\max})$ is the aperture at maximum loading (Eq. (1) evaluated at the maximum stress prior to unloading), and R_m is the recovery ratio (fraction of *mechanical* (not chemical) closure that is recoverable through mechanical–thermal unloading). This relationship implies that gaping of the fracture can only occur through mechanical–thermal elastic relaxation, and not through the chemical processes that influence closure in Eq. (1). The values

Author's personal copy

Table 1
Solid medium properties as used in simulations.

Parameter	Value	Parameter	Value
Bulk modulus of intact rock, $K^{(1)}$ (GPa)	17.0	Volume fraction of fractures (of total reservoir), θ	0.01
Composite bulk modulus, K (GPa)	8.00	Porosity within fractures, ϕ	0.3
Poisson's ratio, υ	0.22	Residual mechanical aperture, b_m^r (μm)	22.5
Bulk modulus of solid grains, $K_s^{(1)}$ (GPa)	54.5	Residual chemical aperture, b_c^r (μm)	20.0
Coefficient thermal expansion, α_T (1/°C)	1.2×10^{-5}	Aperture change constant, β	1.11
Saturated thermal conductivity, λ (W/m K)	2.9	Aperture change constant, χ	345
Heat capacity, C_p (J/kg K)	918	Aperture stiffness constant, ω (1/MPa)	0.20
Porosity of porous media, ϕ	0.02	Mechanical recovery ratio, R_m	0.60

of these parameters as utilized in our simulations appear in Table 1.

Chemical precipitation/dissolution is calculated within TOUGHREACT. The governing equations are described in Taron et al. [1], as presented in the works of Steefel and Lasaga [22] and Xu et al. [23]. Reactions between aqueous species (homogeneous reactions) are assumed to be at local equilibrium, and therefore governed by the relationship between the concentrations of basis (primary) species and their activities, partitioned by the stoichiometric coefficients. This relationship is termed the law of mass action [cf. 22]. The assumption of local equilibrium greatly reduces the number of chemical unknowns and ODE's (between primary and secondary species), and is accurate to the extent that the true reaction rates outpace the rate of fluid transport in a given system. This is a correct assumption for most aqueous species [22] (and flow systems), but less so for slower redox reactions [22,23]. In TOUGHREACT, species activities are obtained from an extended *Debye–Hückel* equation with parameters from Helgeson et al. [24].

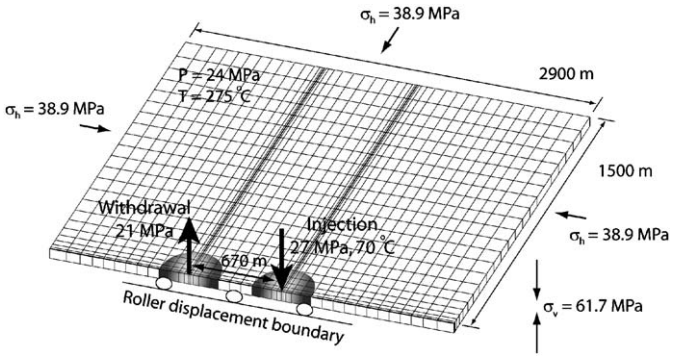

Fig. 1. Initial conditions and geometric layout of EGS reservoir as used in simulations.

4. Model results

In the engineered stimulation of geothermal reservoirs hydraulic, chemical [8,9,25,26], and thermal [27–30] means may be utilized to enhance permeability in a purposeful manner. These stimulations may be used to increase circulation in low permeability systems, and also to counteract future changes that occur as cold water is injected into the reservoir at geochemical disequilibrium. Ideally, injection and withdrawal wells will be connected by a fracture network that is sufficiently permeable to allow rapid fluid interchange, but impermeable enough to allow for sufficiently long thermal residence times in a medium with a large heat transfer area. In addition to achieving an appropriate balance between circulation and residence time, a natural concern arises as to whether unintended stimulations (resulting from critical thermo–hydro-chemical forces of injection) will generate short-circuiting paths between the injection and withdrawal wells via the modification of flow pathways through existing fractures.

Mineral scaling at the wellbore is a known problem, and recent work [e.g. 25,31] indicates that mineral precipitation may also play a large role in reservoir evolution. Moderate success (primarily for calcite) has been achieved in counteracting this through pH modification and the addition of chelatants [8,9]. Chemical changes and the effectiveness of chemical treatments, however, are coupled to hydro-mechanical fracture flow properties. At the Soulz-sous-Forêts geothermal site, for instance, productivity enhancement was observed from chemical treatment at two production wells, but had almost null impact at the injection well, presumably due to the presence of high conductivity fractures that transmitted the treatments quickly away from the problem area [9] and ameliorated their impact. The purpose of this work is to explore the chemical–mechanical couplings responsible for such behaviors and to quantify how strongly they are interlinked.

4.1. Characteristics of simulated EGS

We examine behavior in a prototypical EGS represented by a pseudo 3D doublet geometry of 1500 m × 2900 m, with cold (70 °C) fluid injected through a single well and extracted (670 m away) through a single withdrawal well (Fig. 1). Initially, the reservoir is at 275 °C. Horizontal stresses of 38.9 MPa and a vertical stress of 61.7 MPa are applied at time $t = 0^-$ and allowed to equilibrate with an initial pore pressure of 24 MPa. These conditions are broadly representative of the east flank of Coso geothermal field [32,33]. The lateral boundary that crosses both the injection and withdrawal wells is a plane of symmetry, and as such is restricted to zero displacement in its orthogonal direction (roller boundary). Constant normal stress is held at all other boundaries, and every boundary is thermally insulated and impermeable. The fracture domain is given an initial (unstressed) permeability of 3.0×10^{-11} m^2, and the application of effective stress and temperature at $t = 0^-$ are allowed to decrease this permeability to an *in-situ*, equilibrium value via mechanical closure and pressure solution (assumed to have occurred slowly over geologic time prior to reservoir stimulation). This *in-situ* value is 6.8×10^{-15} m^2 at the given conditions. The granodiorite matrix is given a permeability of 2.0×10^{-18} m^2. Additional properties of the solid medium are shown in Table 1. The injection well operates as a constant source of pressure and temperature equivalent to a well diameter of approximately 12 in, while the withdrawal source serves as a single withdrawal well maintaining a constant pressure at the same diameter. The pressure differential is 3 MPa above and below the *in-situ* value, respectively, and both enter the geometry at the boundary of symmetry.

Author's personal copy

Table 2
Initial volume fraction of reactive minerals in host reservoir.

Mineral	Volume fraction of solid rock[a]	
	Granodiorite	Fractured vein
Anhydrite	–	–
Anorthite	0.33	–
Calcite	0.02	0.31
Chlorite	–	0.23
K-feldspar	0.17	–
Quartz	0.34	0.17
Amorphous silica	–	–

Remaining volume fraction (up to 1) is non-reactive.
[a] From [33].

Reactive composition of the host reservoir rock is presented in Table 2. Calcite and amorphous silica are expected to be the minerals primarily responsible for permeability change due to precipitation and dissolution [cf. 25, 33]. Other likely minerals, such as potassium feldspar and quartz, are also followed, as listed in Table 2. Rate constants for precipitation/dissolution and mineral reactive surface areas of these common minerals are available in the literature, and were utilized as in Xu and Pruess [25]. Calcite and anhydrite are assumed to react at equilibrium (benefiting simulation time by lowering the *Damköhler* number). This assumption is warranted by their very fast relative rate of reaction.

4.2. Mineral precipitation/dissolution

Fluids that are injected into a geothermal reservoir are typically far from geochemical and thermal equilibrium with minerals in the host rock. As minerals precipitate from the injected fluid and dissolve from the rock, changes are incurred in the porosity and permeability of the fracture system. In currently operating geothermal systems, calcite and amorphous silica precipitation have posed problems at recovery and injection wells, respectively. Acidic injection has been shown to successfully inhibit calcite precipitation [8,15]. Aggressive acid–base reactions, however, tend to rapidly dissolve first-contacted minerals and lose effectiveness in the remainder of the wellbore [8]. Other problems with acidification include the potential for corrosion of steel casings, although corrosion inhibitors can often be used. Chelating agents, which reduce the activity of metal ions (through binding), are another alternative for calcite dissolution [9,34] that are suggested to have a less aggressive, more uniform effect [8,34].

Inhibiting the precipitation of amorphous silica has proven more difficult [15]. HF treatment is currently the preferred method, but some have suggested that amorphous silica can be dissolved at high pH with the use of chelating agents to prevent calcite deposition (which would be favored at high pH) [8,34]. This research is, however, relatively recent, and uncertainty remains as to the effects of these treatments on the host rock. Geothermal environments are chemically complex, and field scale results are limited and mixed [9].

In the simulations that follow we present three scenarios for injection fluid composition. Injection water #1 is obtained by extracting the equilibrium, *in-situ* reservoir fluid at 275 °C and allowing it to cool (not in the presence of reactive minerals, as if utilized at the surface with no treatment other than settling) to 70 °C while the aqueous components equilibrate and minerals precipitate. For this injection water, our results show that the injection fluid is not sufficiently saturated with aqueous silica to incur significant reservoir precipitation of amorphous silica, although other minerals are very active. This is a result of the chosen chemistry. As a comparison, field measurements have shown that the precipitation of amorphous silica occurs in fractures at some injection locations in the Coso geothermal field (well 68-20RD), but not at others (wells 68-20, 68A-20, 68A-20RD) [35], depending on the precise injection and *in-situ* chemistry at each well. Two alternative compositions are introduced to examine the behavior of amorphous silica precipitation. Injection water #2 assumes some inefficiency in the surface equilibration process (such as insufficient equilibration time or enhanced dissolution from turbulence) such that only 80% of potential silica precipitation occurs. Simulation #3 is further oversaturated in silica; it represents the potential for rapid chemical change in the reservoir and so assumes that mineral precipitation has been completely restricted during the cool down from 275 to 70 °C (only precipitation is restricted, as primary species are allowed to form secondary species in solution). Injection compositions for each of these cases and for the *in-situ* reservoir are listed in Table 3.

The mineral precipitation/dissolution results of our simulations utilizing these three injection waters are shown in Fig. 2. Fig. 2A compares each injection water for a simulation time of 5 and 20 years for the combined action of all minerals, while Fig. 2B illustrates results for injection water #2 and for each mineral individually. Units are cumulative change in mineral abundance (volume fraction) from time, $t = 0$, such that negative values represent dissolution. Values in Fig. 2B are normalized, such that multiplication of each curve by its normalization magnitude returns the units to cumulative change in mineral abundance. Importantly, water #1 exhibits net mineral dissolution near the injection well (where the cold injection water makes calcite dissolution highly favorable), and net precipitation outside of the thermal reach. This is desirable in the sense that the immediate injection area experiences an increase in permeability, but undesirable in that these dissolved minerals are then re-precipitated as they are heated again between the injection and withdrawal wells. Water #2 changes this behavior in a crucial manner; at 5 years the injection area still experiences net dissolution, but this magnitude is decreased by the precipitation of amorphous silica, and at 20 years the action of amorphous silica has completely erased the positive influence of calcite dissolution. Water #3 shows a more dramatic result, where silica precipitation completely dominates the injection area. This behavior is so pronounced that the simulation was ceased after 7 years due to a complete shutdown of injection permeability ($< 10^{-18}\,\mathrm{m}^2$), and so only the 5 year value is plotted in the figure. One final point regards the magnitude of mineral precipitation outside of the injection area. The higher hydraulic gradient between injection and withdrawal partially outpaces mineral precipitation, such that there is a higher buildup of deposited minerals on the opposite side of injection due to a lower fluid velocity (higher *Damköhler* number).

Further parametric analyses of injection chemistry are not addressed here [cf. 7, 8, 33, 35]. The primary interest in what follows is to present an analysis *not* of specific chemical changes, but of how these changes impact the mechanical system, and how feedback from other permeability altering mechanisms may shift chemical behaviors. We begin by examining the competing magnitudes of chemical vs. hydraulic vs. thermal effects.

4.3. Temporal permeability change

Our model so far attempts to interlink the most important mechanisms in the alteration of reservoir fluid transport properties. This section reverses direction and attempts to extract from

Author's personal copy

Table 3
Fluid chemical compositions (mol/l) used in simulations.

Chemical component	Reservoir fluid	Injection fluid		
		Water #1: initial fracture vein water cooled and equilibrated at 70 °C	Water #2: allowing only 80% completion of SiO_2 precipitation during equilibration to 70 °C	Water #3: restricting all mineral precipitation during equilibration to 70 °C
Al	8.520×10^{-3}	1.894×10^{-8}	1.894×10^{-8}	3.866×10^{-3}
Ca	1.020×10^{0}	1.976×10^{0}	1.976×10^{0}	1.976×10^{0}
Cl	7.420×10^{1}	1.074×10^{2}	1.074×10^{2}	1.074×10^{2}
Fe	4.531×10^{-9}	8.167×10^{-8}	8.167×10^{-8}	8.167×10^{-8}
HCO_3	2.972×10^{-2}	2.010×10^{-1}	2.009×10^{-1}	2.010×10^{-1}
K	6.136×10^{0}	8.413×10^{0}	8.413×10^{0}	8.435×10^{0}
Mg	1.213×10^{-3}	3.938×10^{-3}	3.938×10^{-3}	3.938×10^{-3}
Na	6.359×10^{1}	9.255×10^{1}	9.255×10^{1}	9.255×10^{1}
$SiO_{2(aq)}$	6.210×10^{0}	4.549×10^{0}	4.881×10^{0}	7.856×10^{0}
SO_4	2.766×10^{-2}	7.193×10^{-2}	7.193×10^{-2}	7.193×10^{-2}
pH	6.71	5.82	5.82	5.82

Reservoir composition is at time, $t = 0$. Injection fluid composition remains constant throughout simulation.

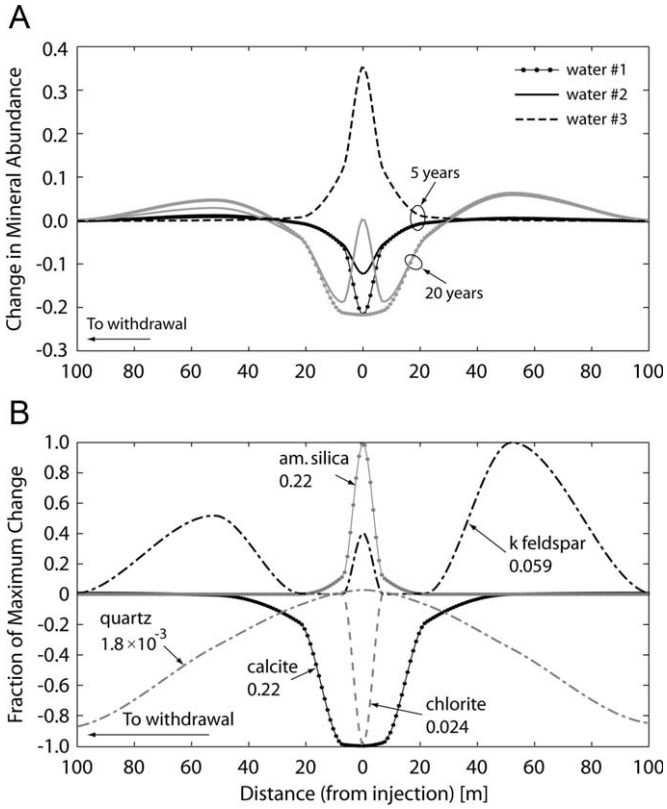

Fig. 2. (A) Change in mineral abundance (all minerals combined) at 5 and 20 years for each of the three injection compositions. Negative values indicate dissolution (decrease in the solid volume fraction) and (B) behavior of each mineral utilizing water #2. Each curve normalized to its own maximum value: Number beneath each mineral indicates the normalizing value (multiply by this number to obtain the true value of each curve).

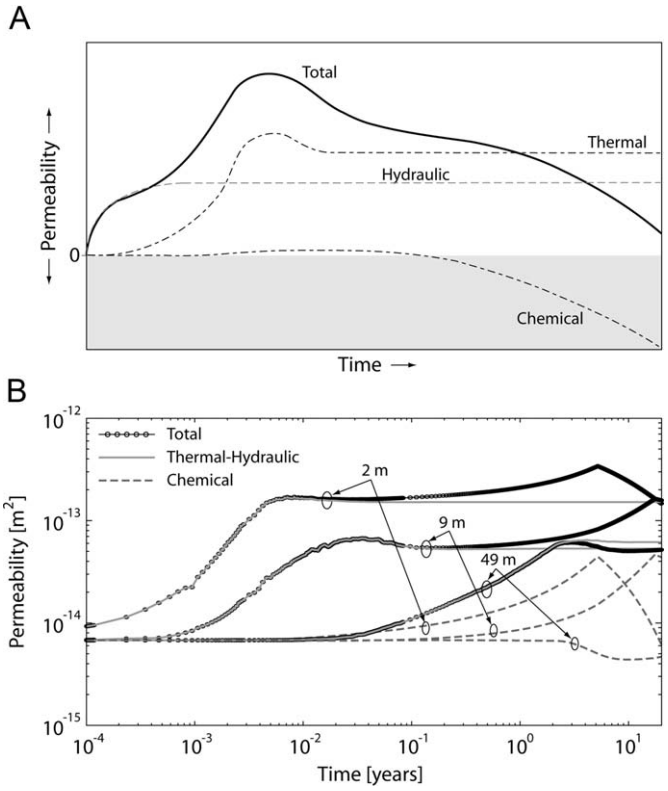

Fig. 3. (A) Conceptual model of permeability altering processes after [26] and (B) contribution of each mechanism to total permeability change in our simulations. Analogous to (A). Changes monitored at 2, 9, and 49 m from injection. Uses water #2.

the coupled analysis the magnitude of influence for each process. It is of interest, both for overall reservoir evolution and for evaluation of potential hydraulic/chemical stimulations, to observe the temporal onset of the various mechanistic causes: In what stages of the lifespan of a geothermal project is thermal (or chemical or hydraulic) forcing the dominant mechanism for change? What measures could then be taken to counteract this, and when should they be applied?

A conceptual model for the possible temporal relationships between THMC processes is shown in Fig. 3A. In a geothermal reservoir subject to cold water injection, hydraulic stimulation should have an immediate effect, tapering off with time to a steady long-term influence. Thermal effects would exhibit a similar trend, but the thermal transfer rate would greatly slow the onset of changes, and there would perhaps be slight reversibility following passage of the thermal front (as adjacent grid blocks contract). Chemical effects should act even more slowly, and perhaps have a dominant influence in the extreme

Author's personal copy

long-term of reservoir life. Mechanical effects are directly active in the first two of these processes—through effective stress and thermal stress.

Simulation results are presented in Fig. 3B in a manner analogous to the conceptual model of Fig. 3A. Aperture change is monitored at three locations in the reservoir (2, 9, and 49 m outward from injection), and each curve at each location represents the contribution of a different process. Total aperture change refers to the contribution from all mechanisms and so reflects the observable change in permeability. Also shown is the contribution to total permeability change due to mineral precipitation/dissolution and TH processes (asperity dissolution via pressure solution and thermal gaping due to cooling). For asperity dissolution/thermal gaping, behavior is conditioned by the combined influence of effective (not total) and thermal stress, and so in this analysis hydraulic and thermal effects cannot be separated (although we present some separation in terms of characteristic times in the following section).

Some clarification is helpful in regard to the two processes implied by TH. In our pressure solution model (see Section 3 and Taron et al. [1]), fracture gaping is not allowed via chemical means ("force of crystallization" is not considered), but only occurs through thermo-mechanical-hydraulic unloading. This behavior, however, is not simply calculated via thermal shrinkage of the matrix blocks, but is handled constitutively as a function of stress reduction and temperature change at the fracture face, and is therefore calculated from the empirical closure relationship (Eqs. (1) and (2)). When the reservoir is loaded, pressure solution is active and instantly (numerically) reduces the reservoir permeability to its "initial" state at loaded conditions (assumed to have occurred slowly over geologic time before stimulation of the reservoir). As the reservoir cools, the matrix contracts and most areas of the reservoir experience thermo-mechanical gaping, while some areas experience an increase in stress and a continuation of pressure solution creep. Both of these actions are controlled by the constitutive relationship, and because thermal gaping is the dominant mechanism during cooling, we refer to both with the TH curves in Fig. 3B.

Mineral precipitation/dissolution is represented by the dashed lines in Fig. 3B. At points near injection, permeability is increased significantly in early times as calcite dissolves into the cool injection water; this behavior is not visible at 49 m from injection. During this time, amorphous silica precipitation counters the dissolution of calcite and decreases permeability, but this behavior is not visible in the plot due to strong dominance from calcite dissolution. As time proceeds, silica is more successful at decreasing permeability and after 5.2 years (2 m from injection) and 17.5 years (9 m from injection) nearly all of the existing calcite within fractures has been dissolved and amorphous silica overrides as a net decreasing trend in permeability. Note that in this simulation calcite dissolves at equilibrium, and that the introduction of kinetic constraints could partially shift the behavior of calcite. At 49 m from injection, only precipitation is significant during the first 20 years of simulation. Note also that neither anhydrite or anorthite is shown in the figure; their contribution is smaller by several orders of magnitude and is focused on the edge of the thermal front $\geqslant$100 m from injection.

Fig. 4 shows contours of permeability and temperature for a reservoir plan-view after 20 years of simulation. Note that the highest permeability is at the injection well, and this tapers off to either side and is surrounded radially by a pocket of lower permeability, particularly to the opposite side of withdrawal. Fig. 5 shows permeability change at a cross section between wells. Note the nearly two order of magnitude variability, and the development of a radial barrier of lower permeability approximately 50 m outward from injection. Fig. 5B illustrates more clearly how this barrier corresponds to the re-precipitation of minerals that are dissolved at injection.

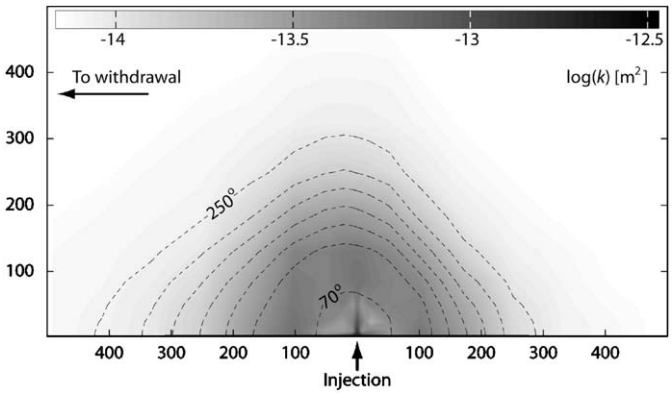

Fig. 4. Plan-view distribution of logarithm of permeability (filled contours) and isotherms (empty dashed contours) at 20 years using water #2. Isotherms increment by 30 °C from 70 to 250 °C.

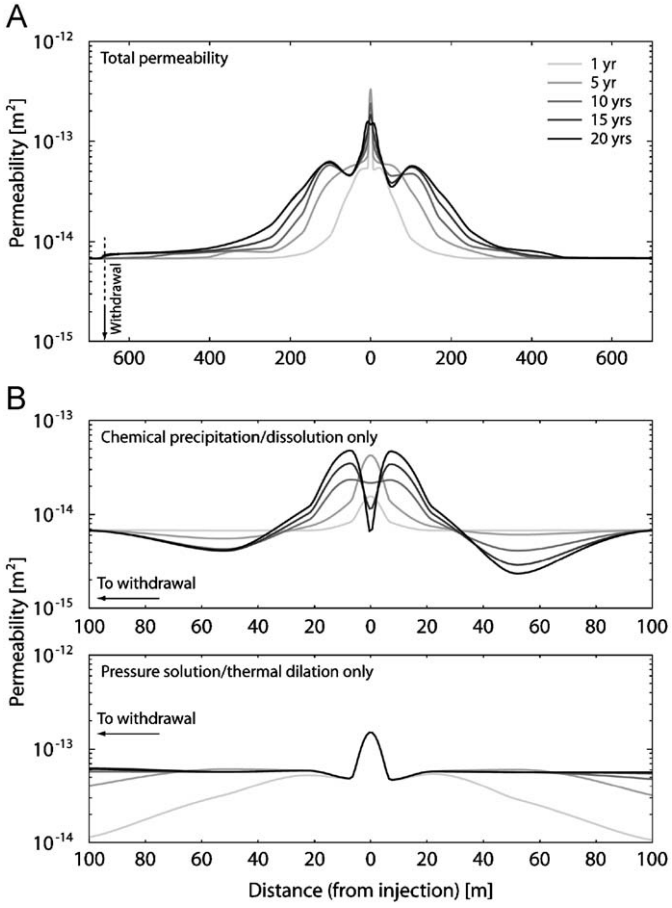

Fig. 5. Permeability changes using water #2: (A) total permeability change with distance from injection and (B) mineral precipitation/dissolution portion and thermal–hydraulic portion of total permeability change in (A). Note the change of scale on the *x*-axis of (B).

4.4. Characteristic times

We can further elucidate the time dependency of competing mechanisms by plotting them vs. their respective characteristic times. We thus introduce the characteristic time, $t_D = ct/l^2$, at a time, t, over the characteristic length scale, l. The diffusivity,

Author's personal copy

c, refers to the ratio of conductivity to capacity/storage, and for thermal conductance is represented by thermal conductivity of saturated rock, λ, density, ρ, and heat capacity, C_p, as $c_T = \lambda/\rho C_p$. When examining the characteristic thermo-elastic response of the reservoir, we note that the timescale of thermal expansion due to a change in temperature will be nearly instantaneous in comparison to the rate of thermal/hydraulic transfer that allows such a temperature change. Hydraulic transport will also influence the thermal characteristic time, such that cooler fluid will be transported via the fracture network to the characteristic location before being thermally conducted into the rock matrix. We conceptualize this process as two conductors in series; thermal characteristic time is recast as $t_D = t \cdot c_{TH}$, where c_{TH} is thermo-hydraulic diffusivity and includes hydraulic and thermal effects as $1/c_{TH} = l_T^2/c_T + l_H^2/c_H$, where the thermal characteristic length scale, l_T, is fracture spacing and the hydraulic length scale, l_H, is the distance of the characteristic location from the injection well. Hydraulic diffusivity, c_H, is discussed below.

Hydraulic effects are characterized by the poroelastic fluid diffusivity, $c_H = k/\mu S$, for permeability, k, dynamic viscosity, μ, and 3D storage coefficient, S (see Wang [36] page 55 for a discussion of storage coefficients), defined as

$$S = \frac{1}{K_v} + \frac{\phi}{K_f}, \tag{3}$$

for the effective porosity of the fractured medium, ϕ, fluid bulk modulus, K_f, and for the solid modulus, $K_v = K + 4/3G$, where K and G refer to the bulk and shear modulus, respectively. Again, the solid response to pressure change is much faster than the rate of fluid conductance, and so the hydraulic poroelastic response is characterized by this hydraulic diffusivity.

For chemical effects, we introduce an analogous relationship. Whereas before we were interested in the ratio of transport to storage, chemical effects depend on the relationship between the rate of chemical reaction and the storage capacity of chemical species in the fracture system. This gives the chemical characteristic time as the ratio of chemical reaction rate to volume capacity of the fractures,

$$t_D = \frac{k_R S_A}{(\theta\phi V/V_M)} \cdot t, \tag{4}$$

for the reaction rate, k_R (in mol/m/s)), total area of precipitation/dissolution (fracture surface area), S_A, volume fraction of fractures in the reservoir, θ, porosity of these fractures, ϕ, characteristic volume scale, V, and molar volume of the mineral species, V_M. We can also rearrange this relationship to produce a "chemical diffusivity" analogous to the above relationships, $c_C = k_R S_A/(\theta\phi h/V_M)$, for reservoir width in the z-direction, h, so that the characteristic time retains its form as $t_D = c_C t/A$, for the characteristic reservoir area, $A = \pi l_c^2$, for the characteristic length, l_c, which is the distance of the characteristic location from the injection well. We thus obtain three characteristic times (and diffusivities) to represent the thermal, hydraulic, and chemical aperture response.

In Fig. 6, four characteristic areas are examined within the influence field of injection; one of 9 m characteristic length (encompassing the area closer than 9 m from injection), one of 24 m, one of 49 m, and one of 129 m, and we take 70 °C (corresponding to the water injection temperature) to be the dominant temperature condition for the life of the project (within these characteristic areas). Water properties correspond to this temperature, and reaction rate is adjusted to this temperature via the Arrhenius expression,

$$k_R = k_{25}\ \exp\left(-\frac{E_a}{R_u}\left(\frac{1}{T} - \frac{1}{298.15}\right)\right), \tag{5}$$

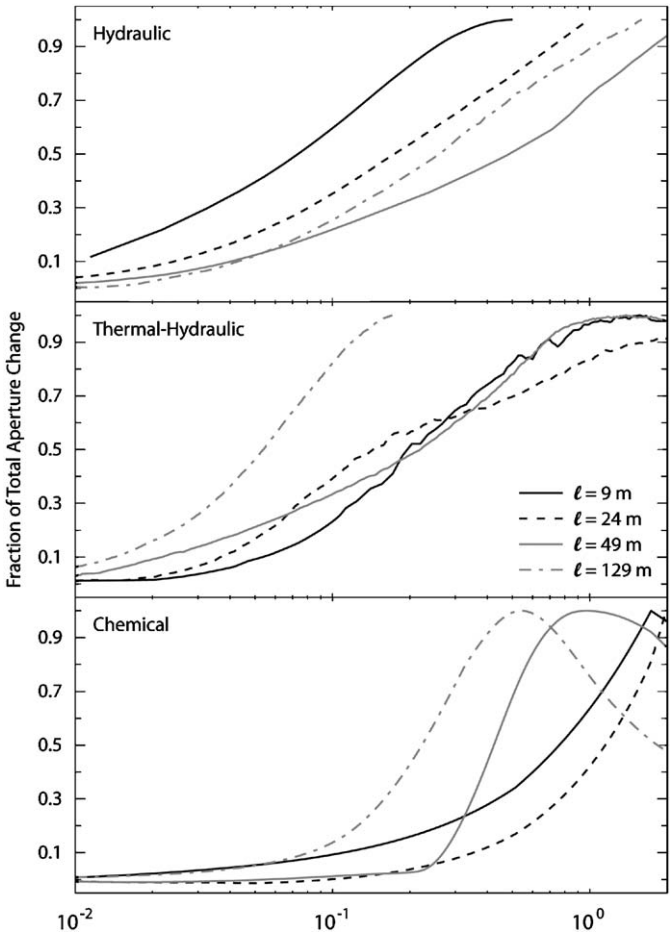

Fig. 6. Characteristic times of permeability change due to hydraulic, thermal–hydraulic, and chemical mechanisms. Changes monitored at 9, 24, 49, and 129 m from injection. Uses water #2.

for the gas constant, R_u, activation energy, E_a, and the rate constant at 25 °C, k_{25}.

As mentioned above, asperity dissolution/thermal gaping behavior is conditioned by effective (not total) and thermal stress and so hydraulic and thermal effects are not directly separable. However, we can focus on hydraulic effects by extracting from the simulation data any changes that occur prior to any noticeable change in temperature; because hydraulic effects are deduced to occur well in advance of thermal arrival. This pre-thermal onset time varies from approximately 10 minutes at 9 m from injection to 4 days at 129 m from injection. Closer than 9 m from injection we are unable to distinguish between mechanisms. Fig. 6 separates hydraulic and thermal effects (both contributing to the empirical aperture change relationship) via this observation, so that data points prior to this shift in behavior are assumed to relate to hydraulic influence (and become the hydraulic curve in Fig. 6). Because the thermal–mechanical relationship includes the effect of hydraulic diffusivity (see above), no separation is required here and the curve is plotted from time, $t = 0$ (this is the true TH curve). To examine characteristic chemical behavior, we adopt for simplicity the rate constant and activation energy of amorphous silica precipitation.

From Fig. 6, we note that for the three plots (hydraulic, TH, and chemical), most of the changes fall characteristically within a timescale of $t_D = 1.2$. Ideally, a curve at any location would overlay perfectly with any other location by characteristic scaling. Given the strong couplings expected between each of the three

Author's personal copy

mechanisms, however, it is perhaps surprising to observe any tendency to follow this ideal, particularly for the TH curves.

In addition to providing a general picture of characteristic reservoir changes, this analysis would seem to have implications for the strength of coupling between each mechanism: a perfect overlay of all curves could indicate a weak coupling. For instance, that TH effects do not significantly influence chemical trends, such that reactive transport simulations at invariant stress would not suffer a penalty in accuracy for this assumption. The following section presents a more direct analysis of this coupling strength.

4.5. Strength of coupling

The primary justification for a THMC modeling strategy is that there exists a strong coupling between chemical and mechanical effects that cannot be represented by parallel reactive transport and geomechanics simulations. In this section we examine the truth of this assertion. We first note that pressure solution can only be simulated with chemo-mechanical coupling, and this alone provides partial justification. However, in the current equilibrium based pressure solution model, coupling to a reactive transport framework is not required (such a linkage may be desirable, but its necessity is currently unclear). Further justification of coupling strength is desirable.

By examination of Figs. 3–5 it is clear that both reactive transport and geomechanical (THMC asperity dissolution/dilation) analysis are required to reproduce the observed order of magnitude changes in permeability; with each causing changes at least as large as one order of magnitude. Furthermore, our pressure solution relationship reduces initial permeability from 3×10^{-11} to $6.8\times10^{-15}\,m^2$ at *in-situ* reservoir conditions (this initial drop is not shown in the figures). Therefore, both of these methodologies are important, and both are required to follow reservoir behavior under these prototypical EGS conditions; but this conclusion does not necessarily imply that they must be interlinked.

Fig. 7 examines this necessity. Fig 6A and B show permeability changes *due only to mineral precipitation/dissolution* (from an initial value of $6.8\times10^{-15}\,m^2$). Two different line styles represent two different simulations; the first utilizes our coupled THMC scheme, and the second operates under invariant stress (no mechanical equilibration and thus no pressure solution or thermal–mechanical dilation). Therefore, differences between the two simulations indicate shifts in mineral precipitation/dissolution behavior that are *caused by changes in the mechanical system*. In Fig. 7A, at 50 m to the left of injection, a reactive transport simulation shows that mineral behaviors cause a reduction in permeability from 6.8×10^{-15} to $5.4\times10^{-15}\,m^2$, while the coupled THMC simulation shows a drop to $2.3\times10^{-15}\,m^2$, or a 3-fold increase in the amount of permeability occlusion, while 10 m to the left of injection shows a 3-fold increase in permeability enhancement. At injection, there is further evidence of this, where amorphous silica precipitates more rapidly in the THMC coupling, resulting in a lower final permeability. Fig. 7B plots these same simulations vs. time, and again illustrates the strong dependence of mineral reactions on mechanical changes.

Fig. 7C and D invert the comparison to examine how changes in the chemical system may alter the evolution of mechanics. Here we plot permeability change *resulting only from* pressure solution/thermo-mechanical gaping, with the same initial value as before. The lines again represent two simulations; one THMC coupled, and a second that does not allow chemical reaction. Therefore, differences between the two simulations indicate shifts in the thermal–mechanical system *caused by changes in the chemical system*. In Fig. 7C we again see shifts in pressure solution/thermal dilation that are caused by precipitation/dissolution, but the coupling is not as strong as for the inverse condition in Fig. 7A. To examine the potential for greater coupling, Fig. 7D conducts the same simulation but utilizes water #3 (more chemically rich). In this case, very large, order of magnitude differences in thermal–mechanical dilation occur when chemical reaction is included.

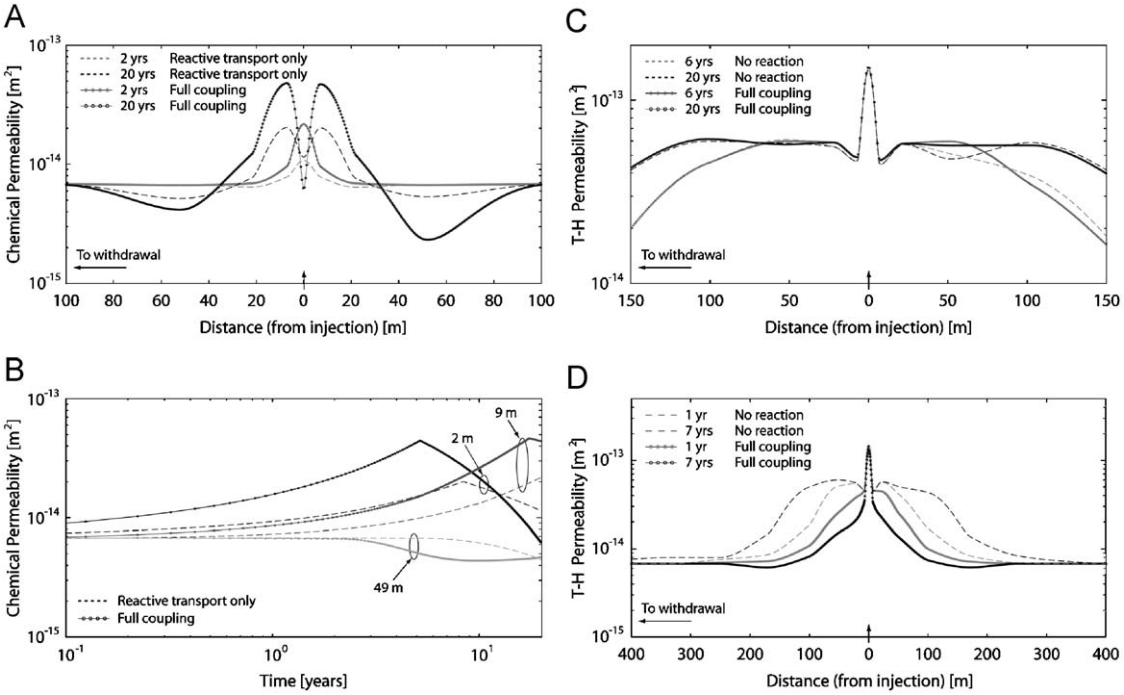

Fig. 7. Permeability comparisons for degrees of coupling: (A) permeability changing due to mineral precipitation/dissolution only: compares full coupling vs. reactive transport alone (invariant stress, no stress dependent aperture change), (B) same as (A) vs. time, (C) permeability changing due to pressure solution/thermal dilation only: compares full coupling vs. exclusion of reactive transport, and (D) same as (D), using water #3 (all others use water #2).

Author's personal copy

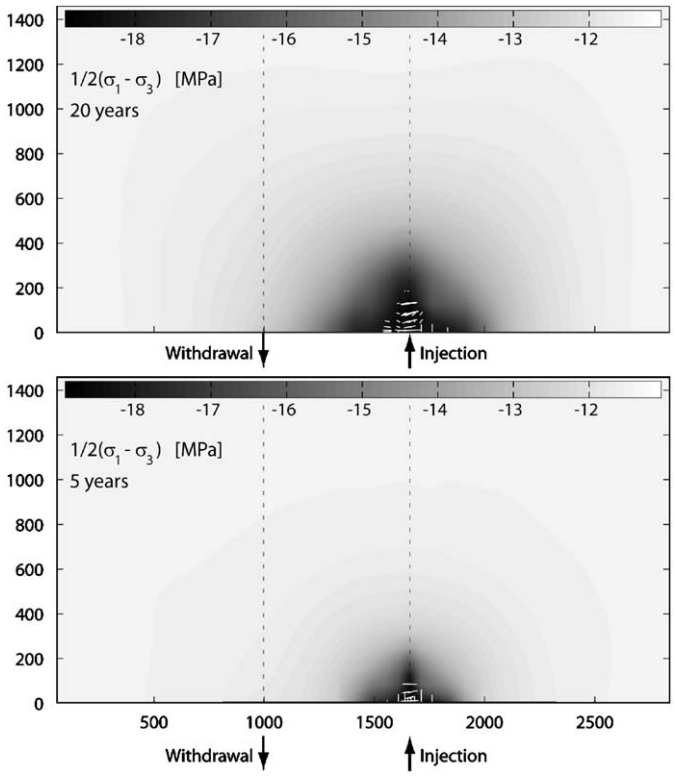

Fig. 8. Plan-view of reservoir with deviatoric stress contours (in MPa) at 5 and 20 years of simulation. White lines are oriented as orthogonal to minimum principal stress direction, and are scaled to the magnitude that shear stress exceeds shear strength.

4.6. Evolution of stress

Deviatoric stress that arises around thermal input can alter fluid circulation and generate a microseismic response. When the deviatoric stress exceeds the bulk strength of reservoir rock or existing fracture planes, permeability may be increased through the dilation and/or extension of existing fractures. This will alter fluid flow paths, and introduce the potential for microseismicity. Fig. 8 follows the advance of deviatoric stress ($\frac{1}{2}(\sigma_1 - \sigma_3)$) with shaded contours. Included on the plot are white vectors to indicate locations where shear stress currently exceeds the reservoir shear strength at that location, and they scale with the excess stress to strength ratio. Their direction indicates the likely direction of failure were it to occur (orthogonal to minimum principal stress). Shear strength is calculated based upon an internal angle of friction of 25° and zero cohesion.

5. Conclusions

A new simulator is utilized to examine dominant permeability altering mechanisms as they relate to critical thermal, hydraulic, mechanical, and chemical behaviors in a prototypical geothermal reservoir. Results demonstrate the strong influence of mechanical effects in the short-term, the influence of thermal effects in the intermediate term, and the prolonged and long-term influence of chemical effects. THMC changes are recast in terms of respective characteristic times, where changes in fracture aperture are shown broadly represented by diffusive timescales representing the respective T, H, and C processes. The potential is evident for permeability alteration of several orders of magnitude due to thermo–hydro-mechanical dilation and chemical precipitation/dissolution. These two processes compete to dominate reservoir behavior; the former controlling the short-term response, and the long-term response characterized by the latter. For the injection of silica saturated water, amorphous silica is capable of drastically reducing permeability close to the injection well. This influence may be countered by the evolution of mechanical shearing in the near-well region, which may exert a strong influence on reservoir and characteristic behavior. Its inclusion into the modeling structure will be the focus of a future work. As an entry point to such an analysis, we have illustrated potential locations for reservoir shear failure by following the evolution of deviatoric stress and its relationship to thermally-derived shear stress.

We have also taken a first step towards the primary justification for a THMC modeling strategy; that there exists a strong coupling between chemical and mechanical effects that cannot be represented by parallel reactive transport and geomechanics simulations. We provide evidence in support of this assertion, illustrating how mineral behaviors alter fluid flow paths and, in so doing, change the characteristics of thermo–hydro-mechanical aperture changes, and vice versa. We show how each incurs changes in the system that fundamentally alter the evolutionary paths of reaction and chemical/mechanical deformation in a manner that decreases the accuracy of conducting the simulations separately.

Acknowledgment

This work is the result of partial support from the US Department of Energy under project DOE-DE-FG36-04GO14289. This support is gratefully acknowledged.

References

[1] Taron J, Elsworth D, Min K-B. Numerical simulation of thermal–hydrologic–mechanical–chemical processes in deformable, fractured porous media. Int J Rock Mech Min Sci 2009; doi:10.1016/j.ijrmms.2009.01.008.
[2] Weyl PK. Pressure solution and the force of crystallization—a phenomenological theory. J Geophys Res 1959;64:2001–25.
[3] Revil A. Pervasive pressure-solution transfer: a poro–visco-plastic model. Geophys Res Lett 1999;26(2):255–8.
[4] Yasuhara H, Elsworth D, Polak A. Evolution of permeability in a natural fracture: significant role of pressure solution. J Geophys Res 2004; 109:B03204.
[5] Paterson MS. Nonhydrostatic thermodynamics and its geologic applications. Rev Geophys Space Phys 1973;11:355–89.
[6] De Boer RB. On the thermodynamics of pressure solution—interaction between chemical and mechanical forces. Geochem Cosmochem Acta 1977;41:249–56.
[7] Xu T, Sonnenthal E, Spycher N, et al. TOUGHREACT—a simulation program for non-isothermal multiphase reactive geochemical transport in variably saturated geologic media: applications to geothermal injectivity and CO_2 geological sequestration. Comput Geosci 2006;32:145–65.
[8] Rose P, Xu T, Kovac KM, et al. Chemical stimulation in near-wellbore geothermal formations: silica dissolution in the presence of calcite at high temperature and high pH. In: Proceedings of the 32nd workshop on geothermal reservoir engineering, Stanford University, 2007.
[9] Nami P, Schellschmidt R, Schindler M, et al. Chemical stimulation operations for reservoir development of the deep crystalline HDR/EGS system at Soultz-Souz-Forêts (France). In: Proceedings of the 32nd workshop on geothermal reservoir engineering, Stanford University, 2007.
[10] Elsworth D, Goodman RE. Characterization of rock fissure hydraulic conductivity using idealized wall roughness profiles. Int J Rock Mech Min Sci 1986;23(3):233–43.
[11] Barton N, Bandis S, Bakhtar K. Strength, deformation and conductivity coupling of rock joints. Int J Rock Mech Min Sci 1985;22(3):121–40.
[12] Wiltschko DV, Morse JW. Crystallization pressure versus "crack seal" as the mechanism for banded veins. Geology 2001;29(1):79–82.
[13] Dewers T, Ortoleva P. Force of crystallization during the growth of siliceous concretions. Geology 1990;18:204–7.
[14] Maliva RG, Siever R. Diagenetic replacement controlled by force of crytallization. Geology 1988;16:688–91.
[15] Tester J, Blackwell D, Petty S, et al. The future of geothermal energy: impact of enhanced geothermal systems (EGS) on the United States in the 21st century. Cambridge, MA: MIT; 2006.

Author's personal copy

[16] FLAC3D Manual: fast Lagrangian analysis of continua in 3 dimensions—version 2.0. Itasca Consulting Group Inc., Minneapolis, MN, 1997.
[17] Settari A. Modeling of fracture and deformation processes in oil sands. In: Proceedings of the fourth UNITAR/UNDP conference on heavy crude and tar sands, paper no. 43, Edmonton, 1988.
[18] Settari A, Mourits FM. Coupling of geomechanics and reservoir simulation models. Comput Meth Adv Geomech 1994:2151–8.
[19] Minkoff SE, Stone CM, Bryant S, et al. Coupled fluid flow and geomechanical deformation modeling. J Pet Sci Eng 2003;38:37–56.
[20] IAPWS, Industrial formulation 1997 for the thermodynamic properties of water and steam. In: International association for the properties of water and steam (IAPWS), 1997.
[21] Min K-B, Rutqvist R, Elsworth D. Chemically and mechanically mediated influences on the transport and mechanical characteristics of rock fractures. Int J Rock Mech Min Sci 2008; doi:10.1016/j.ijrmms.2008.04.002.
[22] Steefel CI, Lasaga AC. A coupled model for transport of multiple chemical species and kinetic precipitation/dissolution reactions with applications to reactive flow in single phase hydrothermal system. Am J Sci 1994; 294:529–92.
[23] Xu T, Pruess K. Modeling multiphase non-isothermal fluid flow and reactive geochemical transport in variably saturated fractured rocks: 1. Methodology. Am J Sci 2001;301:16–33.
[24] Helgeson HC, Kirkham DH, Flowers DC. Theoretical prediction of the thermodynamic behavior of aqueous electrolytes at high pressures and temperatures: IV. Calculation of activity coefficients, osmotic coefficients, and apparent molal and standard and relative partial molal properties to 600 °C and 5 kb. Am J Sci 1981;281:1249–516.
[25] Xu T, Pruess K. Numerical simulation of injectivity effects of mineral scaling and clay swelling in a fractured geothermal reservoir. Report LBNL-55113, Lawrence Berkeley National Lab, Berkeley; 2004.
[26] Rose P. Fracture evolution following a hydraulic stimulation within an EGS reservoir. In: Proceedings of the US DOE EGS program review, 18 July, Golden, CO, USA, 2006.
[27] Nemat-Nasser S, Keer LM, Parihar KS. Unstable growth of thermally induced interacting cracks in brittle solids. Int J Solids Struct 1977;14:409–30.
[28] Pruess K. Enhanced geothermal systems (EGS) using CO_2 as working fluid—a novel approach for generating renewable energy with simultaneous sequestration of carbon. Geothermics 2006;35(4):351–67.
[29] Hunsbedt A, Kruger P, London AL. Recovery of energy from fracture-stimulated geothermal reservoirs. J Pet Technol 1977;29:940–6.
[30] Elsworth D, Xiang J. A reduced degree of freedom model for thermal permeability enhancement in block rocks. Geothermics 1989;18:691–709.
[31] Bächler D. Coupled thermal–hydraulic–chemical modeling at the Soultz-sous-Forêts HDR reservoir (France). PhD dissertation, ETH, Zurich; 2003.
[32] Sheridan JM, Hickman SH. In situ stress, fracture, and fluid flow analysis in well 38C-9: an enhanced geothermal system in the Coso geothermal field. In: Proceedings of the 29th workshop on geothermal reservoir engineering, Stanford University, 2004.
[33] Kovac KM, Xu T, Pruess K, et al. Reactive chemical flow modeling applied to injection in the Coso EGS experiment. In: Proceedings of the 31st workshop on geothermal Reservoir engineering, Stanford University, 2006.
[34] Mella M, Rose P, Kovac KM, et al. Calcite dissolution in geothermal reservoirs using chelants. In: Transactions on geothermal resource council, San Diego, 2006.
[35] McLin KS, Kovac KM, Moore JN, et al. Modeling the geochemical effects of injection at Coso geothermal field, CA; comparison with field observations. In: Proceedings of the 31st workshop on geothermal reservoir engineering, Stanford University, 2006.
[36] Wang HF. Theory of linear poroelasticity. Princeton: Princeton University Press; 2000.